A Gait Monitoring System Based on Air Pressure Sensors Embedded in a Shoe

Kyoungchul Kong, *Student Member, IEEE*, and Masayoshi Tomizuka, *Fellow, IEEE*

***Abstract*—Measurement of ground contact forces (GCFs) provides necessary information to detect human gait phases. In this paper, a new analysis method of the GCF signals is discussed for detection of the gait phases. Human gaits are complicated, and the gait phases cannot be exactly distinguished by comparing sensor outputs to a threshold. This paper proposes a method by fuzzy logic for detecting the gait phases continuously and smoothly. The smooth and continuous detection of the gait phases enables a full use of information obtained from GCF sensors. For advanced rehabilitation systems, this paper also introduces a higher level algorithm that quantitatively monitors the amount of abnormalities in a human gait. The abnormalities detected by the proposed method include an improper GCF pattern as well as an incorrect sequence of the gait phases. To realize the monitoring algorithm, the gait phases are analyzed as a vector and the abnormalities are detected by simple kinematic equations. The proposed methods are implemented by using signals from sensor-embedded shoes called smart shoes. Each smart shoe has four GCF sensors installed between the cushion pad and the sole. The GCF sensor applies an air pressure sensor connected to an air bladder. A gait monitoring system that integrates the proposed methods is shown in this paper and verified for both normal and abnormal gaits.**

***Index Terms*—Abnormality detection, gait monitoring device, human gait phase detection, smart shoes.**

I. Introduction

WALKING is a basic capability that allows humans to pursue their daily lives and function as productive members of society. Walking involves a repetitious sequence of limb motion to move the body forward while simultaneously maintaining stance stability [1]. Walking is characterized by the gait [1]. A typical gait involves one foot placed forward with the second placed the same distance beyond the first. The gait of a normal person, often called the normal gait, is a very efficient gait pattern in terms of power and gait velocity so that a human can walk easily for a long time. Furthermore, the normal gait allows the human to remain agile so that he/she may easily ascend and descent stairs, change walking directions, and swiftly avoid obstacles. Because of these advantages of the normal gait, patients with nervous or muscular disorders strive to rehabilitate and resume the normal gait even though they may have been impaired severely.

Manuscript received April 25, 2008; revised August 14, 2008. First published April 10, 2009; current version published June 17, 2009. Recommended by Technical Editor G. Morel. This work was supported in part by the National Science Foundation under Grant CMMI-0800501.

The authors are with the University of California, Berkeley, CA 94720 USA (e-mail: kckong@me.berkeley.edu).

Color versions of one or more of the figures in this paper are available online at http://ieeexplore.ieee.org.

Digital Object Identifier 10.1109/TMECH.2008.2008803

Modern mechatronics technologies may be utilized in many ways to assist elderly people and patients with walking problems. There have been various rehabilitation devices with monitoring and actuation capabilities installed in hospitals, e.g., LOCOMAT (HOCOMA, Switzerland) [2]. In recent years, active orthoses and exoskeletons to assist patients in their daily lives have been developed, e.g., hybrid assistive limb (HAL, Tsukuba University, Japan) [3], active ankle foot orthosis (Massachusetts Institute of Technology (MIT), USA) [4], and EXPOS (Sogang University, Korea) [5]. In addition, many researchers have studied sensing and biomechatronic technologies to measure and/or estimate the dynamic state of human motions such that these systems can assist humans in more adaptive and interactive ways. For examples, HAL applies electromyography (EMG) sensors to measure muscular efforts [3], and EXPOS applies a novel sensor called a muscle fiber expansion (MFE) sensor [5]. Such methods, however, may not be necessarily the best for applications related to people with physical impairments, because these sensors are based on biological responses in a human body and unreliable in certain patients.

Recently, sensor-embedded shoes have attracted great attention as a sensing device for human motions. For example, Carrozza *et al.* developed an advanced high-level control interface (ACHILLE) based on the sensor-embedded shoes to obtain an appropriate command sequence to control remote devices [6]. Ye *et al.* introduced Shoe-Mouse for hand trauma sufferers to operate computers without hands [7]. Similarly, NoHands-Mouse (Hunter Digital, Inc., USA) is a commercialized foot interface for operating computers with a foot [8]. For the purpose of clinical gait analyses, GaitShoe (MIT) [9] and Intelligent-Shoe (Chinese University of Hong Kong) [10], [11] are noteworthy. The GaitShoe is a wireless sensing device that integrates various sensors, e.g., a triaxial accelerometer, a triaxial gyroscope, four force sensors, etc. The Intelligent-Shoe also utilizes various sensors, such as tilt angle sensors and bending sensors.

In this paper, a sensor-embedded shoe is developed for the use in interactive rehabilitation devices as well as in clinical gait monitoring systems. For such applications, measurement of ground contact forces (GCFs) provides necessary information [4], [12]. Although the GCF signals do not directly provide feedback signals for the control of assistive devices, they do provide a foundation for detecting human motion phases and enable assistive devices to adaptively change the algorithms for each motion phase. For the measurement of GCF, various force sensors have been studied; Kothari *et al.* proposed a capacitive sensor for measuring the pressure between a foot and a shoe [13], and Razian and Pepper developed a triaxial pressure sensor utilizing a piezoelectric copolymer film [14]. The most common

sensor for this application is force-sensitive resistors (FSRs) [7], [9]–[12]. However, the FSRs are not necessarily the best solution due to the low durability and the nonlinearity. In this paper, air bladders are used for measuring GCF, i.e., air bladders are installed in the sole of the shoe, the pressure changes of which are measured by air pressure sensors.

Since the GCF signals do not directly provide information on the dynamic state of a human body, an algorithm that extracts such information from the sensor signals should be introduced. Motion phases during walking are characterized by the gait phases, and each gait phase has a unique GCF pattern. Many approaches have been proposed to detect such gait phases: Pappas *et al.* proposed a pattern recognition algorithm to detect the transitions during the gait cycle based on three FSRs located on an insole and a gyroscope [12] and Huang *et al.* introduced a gait event detection method based on support vector machinery [10]. However, the currently developed methods detect the gait phases as discrete events, while the actual human motion phases cannot be discretely distinguished. Therefore, a smooth and continuous detection method is required for the full use of information obtained from the GCF sensors. The smooth and continuous detection also contributes to a smooth transition of the algorithms in higher level mechatronic devices even in a rapid change of the motion phases. In this paper, a method based on fuzzy logic for smoothly and continuously detecting the gait phases is proposed.

In gaits of certain patients, the GCF patterns are sometimes vague. The gait monitoring algorithm should be able to evaluate the amount of abnormalities in the gait patterns, such that physical therapists can monitor the rehabilitation process quantitatively, and robotic rehabilitation devices can adaptively select a proper control algorithm for each patient. Recently, few algorithms for detecting the abnormalities have been proposed, e.g., Chen *et al.* introduced an abnormal gait detection algorithm based on the frequency-domain analysis [11]. In this paper, a higher level algorithm that monitors the degree of abnormalities in the gait phases detected by the fuzzy logic is proposed. The abnormalities to be monitored by the proposed method include: 1) an improper distribution of the GCF pattern and 2) an incorrect sequence of the gait phases.

This paper discusses the following topics:

1) the design and the verification of a force sensing unit for measuring the GCF in a shoe;
2) the design of an algorithm that smoothly and continuously detects phases in a human gait from the measured GCF;
3) the design of a higher level algorithm that evaluates the amount of abnormalities in the detected gait phases.

The performances are verified by experiments for both normal and abnormal gaits.

This paper is organized as follows. Design of a new force sensing unit to be embedded in a shoe and its signal processing method are introduced in Section II. Section III discusses the fuzzy logic algorithm for smooth and continuous detection of the gait phases. In Section IV, a higher level algorithm that monitors the abnormalities is proposed. The performances of the proposed methods are verified by experiments in Section V. Summary and conclusion are presented in Section VI.

Fig. 1. Shoes with GCF measurement system (smart shoes): air bladders and air pressure sensors are installed for measuring GCFs.

II. Design of Force Sensing Unit

A. Design Concept

The body weight is transferred to feet through bones, and the bones in the feet exert forces to the ground. Due to cushioning materials such as flesh in the sole of the foot and a soft pad in a shoe, the force is distributed over the large area. Therefore, sensors that measure the force in a small area such as FSRs and loadcells are not suitable for measuring the GCFs. Moreover, the practicality of FSRs has not been established from the viewpoints of durability and calibration; for example, Huang *et al.* used a ninth-order polynomial function to compensate for the nonlinearity of FSRs used in the Intelligent-Shoe [10].

In this paper, an air pressure sensor is applied to measure the GCF. A sensing unit is constituted by an air bladder made by winding soft silicone tubes and an air pressure sensor. The end of the tube is tied firmly and bonded by an epoxy adhesive such that it is sealed. Fig. 2 shows the schematic sketch of the proposed sensing unit. When a foot presses the air bladder, it is deformed, and its pressure change is measured by the air pressure sensor. If it is assumed that the radial deformation of the air bladder is constrained and the material of the air bladder has no dynamic effects, the pressure change in the air bladder is proportional to the exerted force, i.e., $P = F/A$.

Requirements of an air bladder are as follows.

1) It causes minimal discomfort.
2) It has reasonable durability under normal loads (i.e., body weight).
3) The range of pressure changes under the normal loads is within the measurable range of an air pressure sensor.
4) It is easy to fabricate.
5) The magnitude of pressure changes is linearly proportional to that of applied forces.

The performance of the proposed sensing unit depends on the characteristics of materials as well as the dimensions of tubes. Various materials are available for tubes, e.g., polyurethane, nylon, Teflon, silicone, etc. However, only nylon and silicone

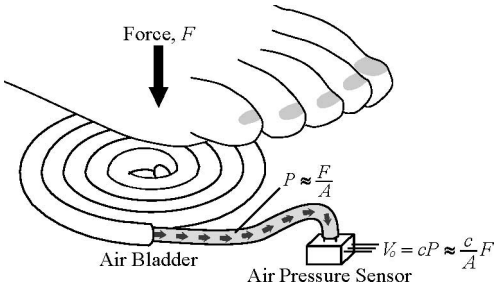

Fig. 2. Schematic sketch of GCF measurement system. F, the force exerted by a foot; P, the air pressure in an air bladder; A, the cross-sectional area of the air bladder; c, a conversion constant of an air pressure sensor; V_O, the voltage output of the air pressure sensor.

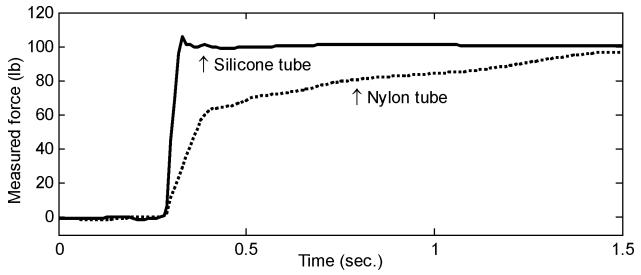

Fig. 3. Step responses of air bladders with silicone and nylon tubes.

tubes were found to be appropriate, because the other materials (e.g., polyurethane and Teflon) are so stiff that they could not be easily mounted under the sole of the shoe. To select the most suitable material among nylon and silicone, the step responses of bladders with silicone and nylon tubes were compared, as shown in Fig. 3. Two air bladders made of nylon and silicone tubes were stacked, and a mass of 100 lb was loaded to examine their performances. As shown in the figure, an air bladder made of nylon tubes showed a large settling time with a creep effect, which implies that the nylon tubes have strong viscoelastic characteristics. Since such characteristics limit the response time of a sensing unit, the silicone tubes were selected for air bladders to measure the GCF in a shoe.

For the first condition discussed before, an air bladder should be thin and flexible, which limits the thickness (i.e., (outer radius − inner radius) of tubes) and the diameter of tubes. However, the tubes should have enough thickness due to the second condition, i.e., thin tubes diminish the durability of air bladders. Table I shows dimensions and test results of some silicone tubes with various sizes. Notice that the pressure change by a mass loaded on an air bladder depends on the diameter of tubes. Since the minimum sensing range of an air pressure sensor [15] is about 0–50 mbar, tubes with the outer diameter of 2 and 3 mm in Table I are not suitable, because the resolution of the sensor cannot be fully utilized. Therefore, the tubes that have the outer diameter of 4 mm and the inner diameter of 2 mm were selected in the design of an air bladder in this paper.

B. Design of Hysteresis Compensator

Fig. 4 shows the performance of the proposed sensing unit. Fig. 4(a) shows the experimental setup. As shown in the figure,

TABLE I
DIMENSIONS OF COMMERCIALLY AVAILABLE SILICONE TUBES

Outer diameter [mm]	Inner diameter [mm]	Required length [mm]	Inside volume [mm^3]	Pressure change* [$m$bar]
2	1	600	470	10
3	1.5	400	710	30
4	2	300	940	50
6	4	200	2500	110
8	6	150	4200	280

*When a mass of 150 lb was loaded on each air bladder.

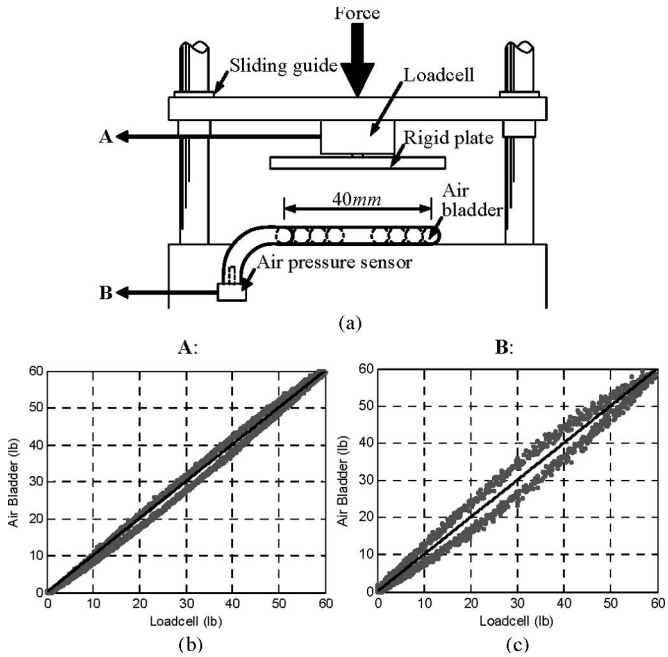

Fig. 4. Linearity tests of the proposed GCF sensing unit. (a) Test setup for verifying performance of the sensor. **A**: measurement by a loadcell. **B**: measurement by the proposed method. (b) At low speed (about 0.1 Hz). (c) At high speed (about 1 Hz).

an air bladder and a loadcell are in series such that they measure the same force. At the loadcell, a large rigid plate was attached to apply a distributed force to the air bladder. To make sure that the two sensors are in series, the upper plate was constrained by frictionless guides. Even though this configuration is not realistic because a human foot does not necessarily exert only normal forces, the experimental setup shown in Fig. 4(a) was designed to precisely verify the performance of sensors. The force was exerted by pushing the upper plate. Assuming that the loadcell is ideal, it is desired that the loadcell and the proposed method measure the same values regardless of the magnitude and the speed of the applied force. The loadcell used in the experiments is an FC21 model of Msisensors Company [16]. Its performance was verified before this experiment. Fig. 4(b) shows the relation between measurements of the loadcell and the proposed method for a low-speed exertion. Note that it is close to linear. When the applied force is rapidly changed, however, the proposed method shows a large hysteresis, as shown in Fig. 4(c), which implies that the dynamic characteristics of the air bladder cannot be neglected.

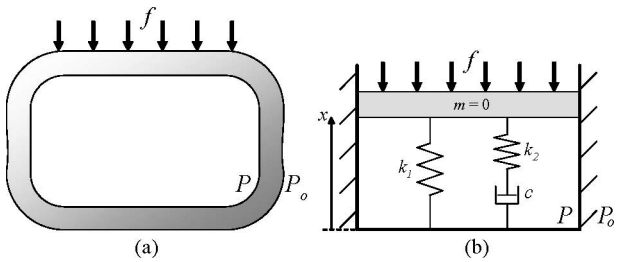

Fig. 5. Air bladder model. (a) Silicone tube model. (b) Simplified model.

TABLE II
SOME PHYSICAL PROPERTIES OF AIR BLADDER

Property	Quantity
Effective cross-sectional area, A	$4.7124\times10^{-5}[m^2]$
Inside volume when undeformed, Ax_0	$9.4248\times10^{-8}[m^3]$
The number of moles, n	4.2075×10^{-9}[mol]
Universal gas constant, R	8.3145 [m^3PaK^{-1}mol^{-1}]
nRT at T=300K	1.0494×10^{-5}[Pa m^3]

To compensate for the hysteresis effect, the air bladder is modeled, as shown in Fig. 5. Modeling of the silicone tube is to compensate for such effect by treating it as a viscoelastic effect of the material. Therefore, a model that describes viscoelastic materials [17], which consists of two springs and a damper, as shown in Fig. 5(b), is applied to represent the silicone tube. It is assumed that the tube has no air leakage and no inertia, i.e., $m = 0$. In Fig. 5, P_o and P represent the atmosphere pressure and the absolute pressure in the tube, respectively. The parameter f is the applied force and distributed over the large area.

The force balance equation for the model in Fig. 5(b) is

$$PA - P_O A - fA - \left[k_1 + \frac{k_2 cs}{k_2 + cs}\right](x - x_0) = 0 \qquad (1)$$

where A is the effective area of the air bladder and the other parameters are as shown in Fig. 5. Note that (1) is in the Laplace domain, where s in (1) refers to a derivative operator. After a transfer function from the applied force to the output signal is obtained based on the Laplace domain analysis, it will be converted into a transfer function in the discrete-time domain for implementation in a digital processor. The ideal gas state equation is

$$P = \frac{nRT}{Ax} \qquad (2)$$

where the parameters are defined in Table II. If the deformation is small, i.e., $x - x_0 \approx 0$, where x_0 is the inside height of the undeformed tube, (2) is approximated as

$$P = \frac{nRT}{A}\left[\frac{1}{x_0} - \frac{(x - x_0)}{x_0^2}\right]. \qquad (3)$$

Note that the first term on the right-hand side is the pressure in the air bladder when it is not loaded, i.e., $nRT/Ax_0 = P_0$. Defining a gauge pressure as $P_G \equiv P - P_0$, (3) is

$$(x - x_0) = -\frac{Ax_0^2}{nRT} P_G. \qquad (4)$$

Substituting (4) into (1), the governing equation is expressed as a function of the gauge pressure P_G, i.e.

$$f = P_G + \left[k_1 + \frac{k_2 cs}{k_2 + cs}\right]\frac{x_0^2}{nRT} P_G \equiv \frac{b_1 + b_2 s}{a_1 + a_2 s} P_G \qquad (5)$$

where

$$a_1 = k_2, \qquad a_2 = c \qquad (6)$$

$$b_1 = k_2\left[1 + k_1\frac{x_0^2}{nRT}\right], \quad b_2 = c\left[1 + (k_1 + k_2)\frac{x_0^2}{nRT}\right]. \qquad (7)$$

In (5), P_G is measured by a pressure sensor and f is to be estimated. Note that if the viscoelastic effect of material is weak (i.e., $k_1 = k_2 = c \approx 0$), the transfer function from P_G to f is close to one, i.e., no signal processing is required. If the material is very stiff (i.e., $k_1 \gg 0$), the gain of the transfer function is very large such that the sensor noise is amplified. Also, since the pole and the zero of the transfer function are negative (i.e., $-a_1/a_2 < 0$ and $-b_1/b_2 < 0$), the signal does not show a drift. This holds only when the tube has no leakage. It should also be noted that the magnitude of the pole is greater than that of the zero (i.e., $|a_1/a_2| > |b_1/b_2|$), and thus, the transfer function magnifies the high-frequency range of the measured signal.

The authors have noted so far that the silicone tube used in this paper has proper characteristics in terms of stiffness as well as durability, but that its viscoelastic characteristics cannot be neglected, as shown in Fig. 4. Therefore, the signal is to be filtered by the transfer function in (5), which is obtained by a physical model. Since k_1, k_2, and c in (6) and (7) are unknown, they are obtained by the curve-fitting method such that the filtered signal is linearly proportional to the measurement of the loadcell. For implementing the transfer function in (5) in a digital processor, it is converted into the discrete-time domain by the Euler method, i.e.

$$f(k) = c_1 f(k-1) + c_2 P_G(k) + c_3 P_G(k-1) \qquad (8)$$

where c_1, c_2, and c_3 are $a_2/(a_1 dt + a_2)$, $(b_1 dt + b_2)/(a_1 dt + a_2)$, and $-b_2/(a_1 dt + a_2)$, respectively. The variable dt is the sampling period of the digital processor. Note that (8) is a digital IIR filter, the frequency response of which is close to that of (5).

Fig. 6 verifies the compensation performance. Fig. 6(a) is the frequency response of the filter obtained by the curve-fitting based on the transfer function in (5). Note that it has a magnifying characteristic in the high-frequency range with a phase lead. Due to the phase lead, the time delay caused by the viscoelastic characteristics is compensated. Fig. 6(b) shows the linearity between the filtered signal and the loadcell measurement. Even though the sensor noise was amplified slightly, the filtered signals show a good linearity without hystereses. The filtered signal has the noise level of 1.5 lb in root mean square. Since it is less than 1% of body weight, the proposed sensor is considered to be suitable for measurement of the GCFs.

C. Repeatability

Since a human gait is repetitious, the GCF is also repetitive and the sensing unit should have a good repeatability. The repeatability is defined by the variation of measurements taken

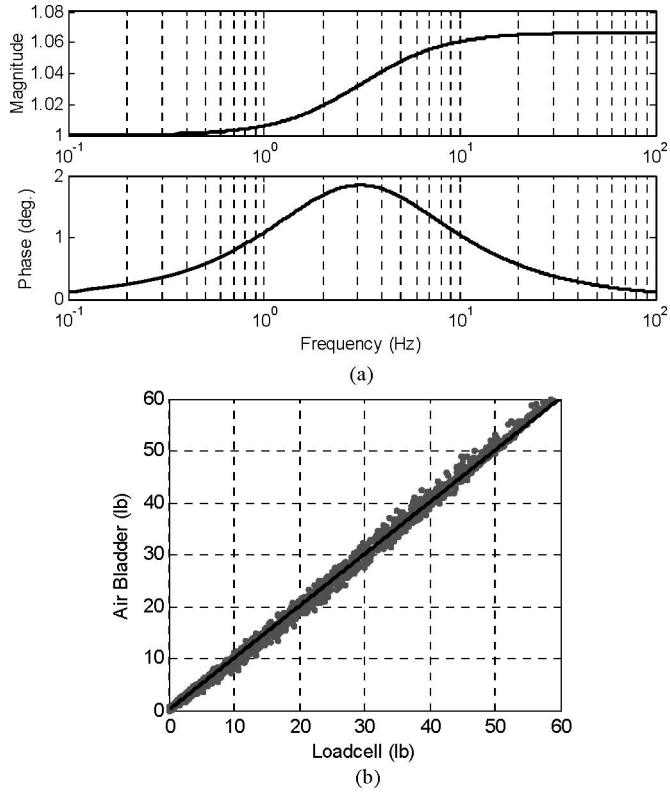

Fig. 6. Signal compensation based on a physical model. (a) Frequency response of the filter obtained by curve fitting. (b) Compensated signal [the raw signal is shown in Fig. 3(c)].

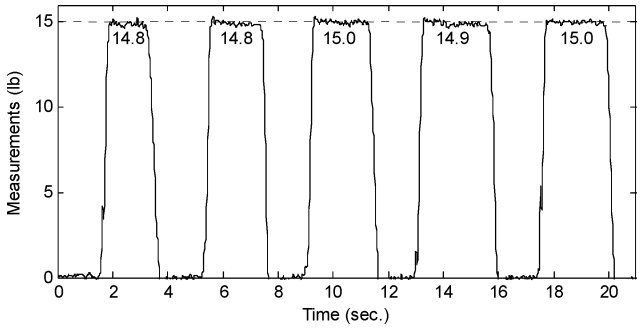

Fig. 7. Repeatability test.

by several experiments under the same conditions. To verify the repeatability, the experimental setup in Fig. 4(a) was used where the force was applied by repetitively putting a mass of 15 lb. Fig. 7 shows the experimental results. In the figure, the signals obtained by the proposed sensing unit were processed by the filter shown in Fig. 6(a). The numbers in the figure represent the average values of steady signals. They are desired to be the same for each experiment. Note that the proposed sensing unit shows a good repeatability (>97%).

D. Implementation of Sensors in Shoe

The proposed sensing unit is implemented in a shoe, as shown in Figs. 1 and 8. The weight of each sensing unit including an air bladder and an air pressure sensor is less than 20 g such that

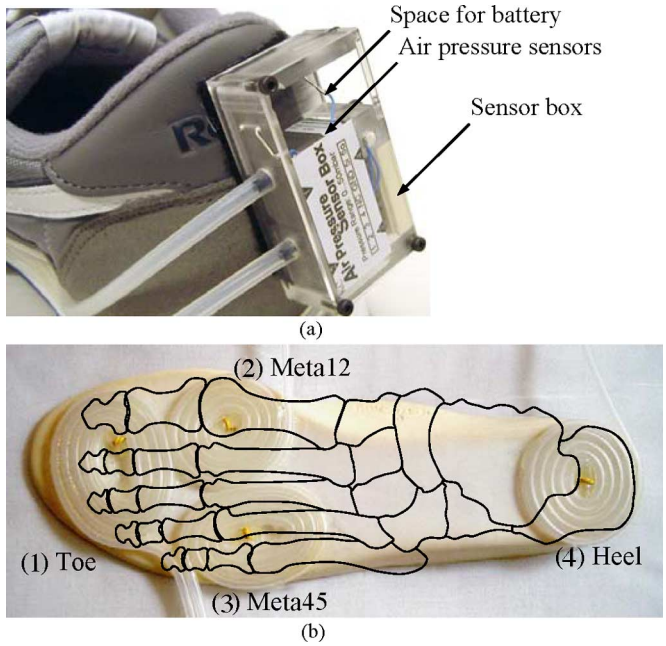

Fig. 8. Implementation of the proposed GCF sensing unit. (a) Sensor box that includes four air pressure sensors. (b) Sole of the smart shoe with four air bladders. Meta12 and Meta45 refer to the first and second, and the fourth and fifth metatarsophalangeal joints, respectively.

it may cause minimal changes on human motions. In a shoe, four air bladders and four air pressure sensors are installed, and each pair is connected independently.

Air pressure sensors used in this paper are the BSDX model of Sensor-Technics Company [15] that has the sensing range of 0–50 mbar and a built-in amplification circuit. It is packaged in a sensor box, as shown in Fig. 8(a). Air bladders are located based on anatomical information. Although the force is distributed by the flesh, the maximum force still occurs at the location of the bone. Therefore, it is reasonable to locate sensors at joints of bones in the foot. Four air bladders are installed under the sole of a shoe, as shown in Fig. 8(b). To measure the GCF pattern more precisely, five air bladders may be placed at the regions of (2) and (3) in Fig. 8(b), but practically two bladders are enough to distinguish the GCF patterns, because those joints are strongly connected to each other by muscles. It should be noted that the proposed method is less sensitive to the change of the foot shapes compared to FSRs due to its large sensing area.

III. Smooth and Continuous Detection of Gait Phases

A. Motion Phases in Human Gait

To provide the basic functions required for walking and to minimize its required energy, walking motion involves unique patterns called gait phases. The human gait is usually divided into eight functional patterns developed by the Rancho Los Amigos gait analysis committee [1]. In Fig. 9, GCF patterns corresponding to different gait phases are shown. The swing phase consists of three phases: initial swing, mid-swing, and terminal swing phases. Since a leg in the swing phase does not

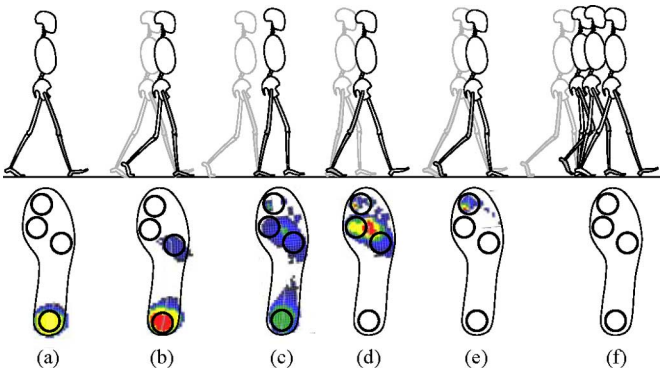

Fig. 9. Fundamental gait phases of a leg (shaded) [1] and their associated GCF patterns in the right foot. (a) Initial contact. (b) Loading response. (c) Mid stance. (d) Terminal stance. (e) Preswing. (f) Swing.

touch the ground, the three phases may not be distinguished by the GCF patterns. Therefore, they are combined into one phase in Fig. 9(f), and a gait is analyzed with the six phases in this paper. This is acceptable for most of the applications including assistive devices, because physical models of the leg in the swing phases are identical (e.g., double pendulum [24]).

B. Detection of Gait Phases by GCF Measurements

A simple and naive way to detect the gait phases shown in Fig. 9 would be to apply a threshold to the GCF measurements. The threshold method is effective when changes of the signal are very distinct, e.g., a digital signal. Normally, GCF in feet, however, changes smoothly and continuously to protect joints from impact forces. When it is measured by force sensors in shoes, it may be more smoothened due to the flesh as well as the cushioning materials in the sole of the shoe.

For this purpose, fuzzy logic is suitable. In the case of fuzzy logic, a human gait is analyzed as a set of whole gait phases, where the likelihood of each gait phase is determined by each fuzzy membership value (FMV, μ). For example, when an FMV of a gait phase is close to one, the leg of which GCF pattern is measured is quite likely in the phase. If FMVs of two phases are about 0.5 at the same time, the leg may be in a transition between the two phases.

The fuzzy logic method is useful when a set of rules is established based on a sound understanding of the problem. The rules for the gait analysis are established based on the expected GCF pattern shown in Fig. 9. For example, only heel is expected to show a large GCF in the initial contact phase [see Fig. 9(a)], and therefore its likelihood (i.e., $\mu_{\text{initial contact}}$) is close to one only if the heel shows a large GCF while the others are small. Table III shows a set of the rules for detecting the six gait phases shown in Fig. 9. In the table, some ambiguous conditions are ignored and marked by N/A.

Before implementing the rules in Table III, two major questions remain: 1) how large is "Large" or how small is "Small" and 2) how the rules are interpreted in programmable logics. The first question is equivalent to how to design membership functions in the fuzzy logic. In this paper, a membership function that applies the hyperbolic tangent function is used, i.e.

TABLE III
FUZZY RULE BASES FOR GAIT ANALYSIS

				Fuzzy Membership Value
Large	Small	Small	Small	$\mu_{Initial\ Contact} \rightarrow 1$
Large	Large	Small	Small	$\mu_{Loading\ Response} \rightarrow 1$
Large	Large	Large	N/A	$\mu_{Mid\ Stance} \rightarrow 1$
Small	Large	Large	N/A	$\mu_{Terminal\ Stance} \rightarrow 1$
Small	Small	Small	Large	$\mu_{Pre-Swing} \rightarrow 1$
Small	Small	Small	Small	$\mu_{Swing} \rightarrow 1$

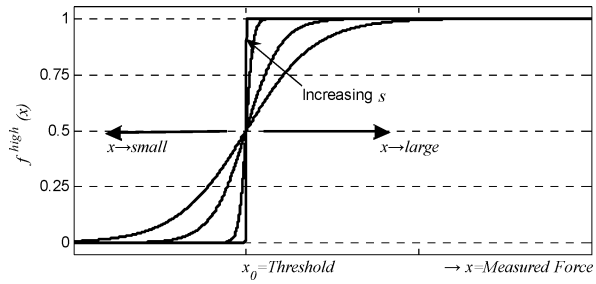

Fig. 10. Fuzzy membership function.

$$f^{\text{Large}}(x) = \frac{1}{2}\left[\tanh(s(x - x_0)) + 1\right] \in [0, 1] \tag{9}$$

where x, x_0, and s represent the measured GCF, the threshold value, and the sensitivity coefficient, respectively. The membership function in (9) has the following benefits.

1) It is continuous and smooth over the entire range: This contributes to continuity and smoothness of the resultant outputs of the fuzzy logic.
2) It is a symmetric function, such that the contra membership function is simply obtained by

$$f^{\text{Small}}(x) = 1 - f^{\text{Large}}(x) \in [0, 1]. \tag{10}$$

This reduces the calculation time in real-time applications.
3) It returns 0.5 when the measured GCF is equal to the threshold: Intuitively this is reasonable since the threshold value means neither large nor small.
4) It is easy to adjust the sensitivity: By adjusting one parameter s, the slope of the membership function changes without loss of other characteristics stated before. The slope of the membership function is

$$\frac{df^{\text{Large}}(x)}{dx} = \frac{1}{2}s[1 - \tanh^2(s(x - x_0))]. \tag{11}$$

Note that (11) is equal to $0.5s$ at the threshold value, i.e., $x = x_0$. As s increases, the membership function becomes more distinct but more sensitive to the selection of the threshold value. It should also be noted that the membership function is asymptotic to the one for the crisp logic as $s \rightarrow \infty$. Fig. 10 shows the shape of the membership function of (9) for various s.

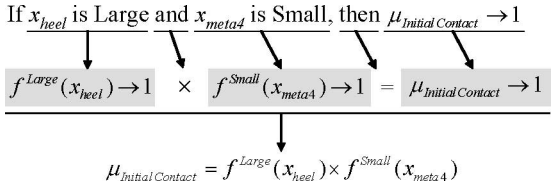

Fig. 11. Mathematical interpretation of the rule for the initial contact phase.

To accomplish the mathematical implementation of the fuzzy rules in Table III, the Larsen product implication method [18] is used as the inference operator. Fig. 11 shows how the rules in Table III are converted to mathematical expressions in the case of the initial contact phase. The other phases follow the same logic. The statement of "x is Large" is equivalent to "$f^{\mathrm{Large}}(x) \to 1$." It should be noted that each FMV is close to one only if its all conditions are satisfied. For more detailed information on fuzzy logic, see [19].

It is desired that each FMV represents the likelihood of each gait phase. For this purpose, a scaling factor *sf* is introduced to make the summation of all FMVs one for all the time, i.e.

$$sf(k) = \frac{1}{\sum \mu_i(k)} \tag{12}$$

where k represents a time index and $\mu_i(k)$ is the FMV of each gait phase, i.e., $\mu_1(k) = \mu_{\mathrm{initial\ contact}}(k)$, $\mu_2(k) = \mu_{\mathrm{loading\ response}}(k)$, etc.

Fig. 12 shows the entire fuzzy logic. Information in each step is manipulated and passes into the next step by applying the methods shown in Fig. 12. Arrows represent the signal flow and all steps are realized in one sampling time. The gait phases are analyzed for each foot, so that the equivalent algorithm is applied to both feet at the same time to observe the whole phases in a human gait.

IV. Detection of Abnormalities in Gait Phases

The GCF patterns in an abnormal gait may be different from those in a normal gait and serve as the information source to detect abnormal gait phases. The abnormality can be defined by two major conditions: 1) when the current GCF pattern cannot be explained by the desired patterns in a normal gait and 2) when the sequence of the gait phases obtained by analyzing the GCF patterns is incorrect. Using the smart shoes proposed in this paper, both abnormalities are monitored by an algorithm built on top of the fuzzy logic.

A. Detection of Abnormalities in GCF Patterns

The scaling factor in (12) provides information on the amount of abnormalities in a gait at a given time. Intuitively, the scaling factor should be one if all parameters in the fuzzy logic are adequate, and a subject has the normal gait as defined in Fig. 9. When the scaling factor is less than one, it means that more than one gait phase is detected (note that $\mu \in [0, 1]$). If it is greater than one, no expected GCF pattern in Fig. 9 exactly matches the current pattern. In addition, since the scaling factor is a time function as defined in (12), it may indicate in which

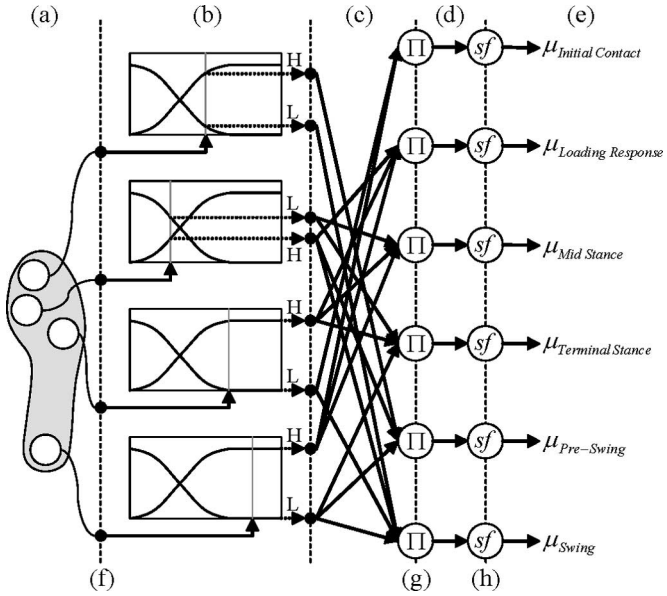

Fig. 12. Overall fuzzy logic for detection of gait phases. (a) Pressure changes in air bladders. (b) Fuzzy membership functions defined in (9). (c) Fuzzy rule bases (Table II). (d) Unscaled outputs. (e) Outputs of fuzzy logic. (f) Air pressure sensors. (g) Inference operator (Fig. 11). (h) Scaling factor defined in (12).

phase the subject has a problem. It should be noted that since this method measures the abnormality by monitoring the sum of FMVs at a given time, it does not necessarily detect all of the abnormalities, e.g., the time sequence of gait phases can be incorrect even though the scaling factor is one for all the time.

B. Detection of Abnormalities in Gait Phase Sequences

In a normal gait pattern, the phases shown in Fig. 9 appear sequentially. Otherwise, the walking motion is unnatural and is characterized by an abnormal gait. For example, a patient dragging his/her foot may miss the swing phases, i.e., the leg shows the initial contact phase after the preswing phase. Therefore, another abnormality is observed by monitoring the sequence of gait phases.

A simple method to check the sequence of the gait phases is applying a discrete event analysis constituted by some "if and then" logics. In this paper, a more mathematical method is proposed to quantitatively monitor the sequential abnormality.

For simplicity, suppose that a human gait has three phases, i.e.

$$\begin{aligned}\vec{y}(k) &= [\,\mu_1(k) \quad \mu_2(k) \quad \mu_3(k)\,]^{\mathrm{T}} \in \Re^3 \\ &= \sum_{i=1}^{3} \mu_i(k)\vec{e}_i \end{aligned} \tag{13}$$

where $\vec{y}(k)$ represents a gait phase vector at time k, $\vec{e}_i$ is an orthonormal basis vector in the Cartesian coordinate, and $\mu_i(k)$ is the FMV of each gait phase. Since each gait phase appears sequentially in a normal gait, each component in $\vec{y}(k)$ is expected to show a large value sequentially, i.e., $\mu_1 \to \mu_2 \to \mu_3 \to \mu_1$, and so on. Fig. 13 shows a graphical representation of the gait phase vector and its movement in normal gait cases. Note that

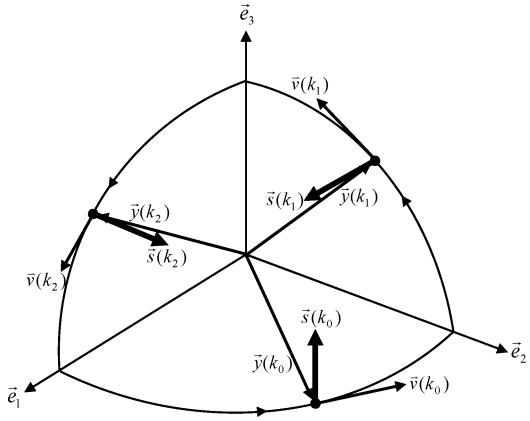

Fig. 13. Graphical representation of the gait phase vector in a 3-D case.

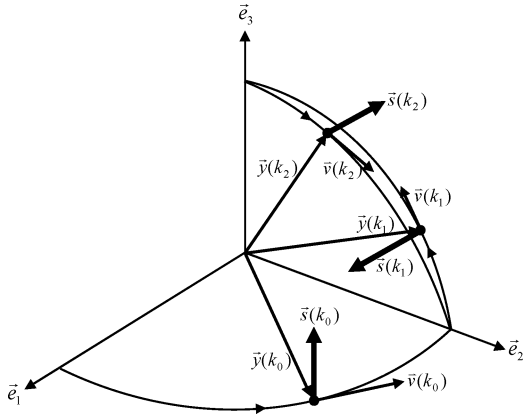

Fig. 14. Graphical representation of the gait phase vector in an abnormal case.

$\vec{y}(k)$ rotates in a certain direction. For example, in the figure, $\vec{y}(k)$ is in e_1–e_2 plane and moving toward the $\vec{e}_2$-axis at k_0. It is in e_2–e_3 plane and moving toward the $\vec{e}_3$-axis at k_1. In the figure, $\vec{v}(k)$ represents a tangential vector of the gait phase vector, i.e.

$$\begin{aligned}\vec{v}(k) &= \vec{y}(k) - \vec{y}(k-1) \\ &= \sum_{i=1}^{3} \Delta\mu_i(k)\vec{e}_i \end{aligned} \tag{14}$$

and $\vec{s}(k)$ is their cross product, i.e.

$$\vec{s}(k) = \vec{y}(k) \times \vec{v}(k). \tag{15}$$

In the 3-D Cartesian space, $\vec{s}(k)$ is always perpendicular to both $\vec{y}(k)$ and $\vec{v}(k)$. Moreover, if $\vec{y}(k)$ moves, as shown in Fig. 13, components of $\vec{s}(k)$ are nonnegative always. In other words, $\vec{s}(k)$ has a negative component if any of the phases is missing or does not move as expected. Therefore, based on the direction of $\vec{s}(k)$ [i.e., by checking the negative components of $\vec{s}(k)$], the abnormalities in the gait phase sequence are monitored.

Fig. 14 shows an abnormal case in the three-phase problem. In the figure, the gait phase vector normally moves from $\vec{e}_1$ to $\vec{e}_2$ at k_0, and from $\vec{e}_2$ to $\vec{e}_3$ at k_1. However, it moves back to $\vec{e}_2$ at k_2, which implies that μ_2 appears after μ_3 missing μ_1. Since this is an abnormal case, it should be detected by the algorithm. Notice that the cross product vector indicates $-\vec{e}_1$ direction at k_2. Therefore, such abnormal case can be detected by checking the negative component in the cross product in (15).

The fuzzy logic detects six phases as defined in Table III. Therefore, the gait phase vector $\vec{y}(k)$ is 6-D in actual cases, and its tangential vector $\vec{v}(k)$ also has six components. We have utilized the orthogonality of a cross product operator to detect phase transitions in a three-phase problem, but such characteristic of the cross product does not hold for six-phase problems [20]. Thus, the logic proposed earlier is not directly applied to the gait phase problem.

This problem is solved by defining some dummy variables. For example, a dummy variable is defined by adding four FMVs as

$$d_1(k) = \mu_3(k) + \mu_4(k) + \mu_5(k) + \mu_6(k). \tag{16}$$

Note that $d_1(k)$ is always less than or equal to one because the summation of all scaled FMVs are one for all k. In other words, $d_1(k)$ has the same characteristics as the FMV. A new gait phase vector is defined using the dummy variable, i.e.

$$\vec{y}_1(k) = [\,\mu_1(k) \quad \mu_2(k) \quad d_1(k)\,]^{\mathrm{T}} \in \Re^3. \tag{17}$$

Applying the same logic, it is possible to monitor the sequence of two phases. Similarly, two more gait phase vectors are defined as

$$\vec{y}_2(k) = [\,\mu_3(k) \quad \mu_4(k) \quad d_2(k)\,]^{\mathrm{T}} \in \Re^3 \tag{18}$$

$$\vec{y}_3(k) = [\,\mu_5(k) \quad \mu_6(k) \quad d_3(k)\,]^{\mathrm{T}} \in \Re^3 \tag{19}$$

where

$$d_2(k) = \mu_1(k) + \mu_2(k) + \mu_5(k) + \mu_6(k) \tag{20}$$

$$d_3(k) = \mu_1(k) + \mu_2(k) + \mu_3(k) + \mu_4(k). \tag{21}$$

V. Implementation and Experiments

In this section, the proposed methods for detecting abnormalities and gait phases are verified by experiments.

A. Implementation

The final goal of the proposed research is the design of a mobile and real-time gait monitoring system that can be utilized for intelligent rehabilitation devices. The algorithms and the sensor-embedded shoe serve as the basic sensor and signal processor such that higher level algorithms, such as long-term rehabilitation programs, can utilize the information. For this purpose, the proposed algorithms are implemented in a digital mobile processor, which can be carried by a patient, and the processed data are transferred to a host computer, where the higher level algorithms may be running.

Fig. 15 shows a possible implementation of the proposed methods. Considering the computation capability of a processor, CompactRIO of National Instruments [21] was utilized in

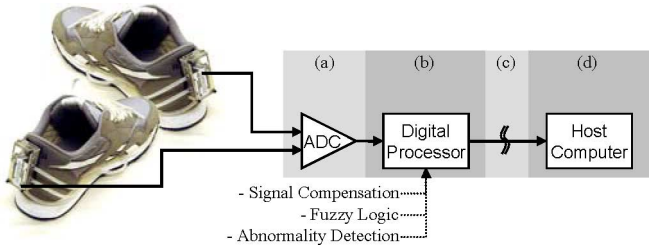

Fig. 15. Implementation of smart shoes.

TABLE IV
OUTPUTS OF PROPOSED GAIT MONITORING SYSTEM

Description	No. of outputs per each foot	No. of outputs for both feet
Ground contact forces[1)]	4	8
Likelihoods for gait phases[2)]	6	12
Scaling factor in fuzzy logic	1	2
Components of cross products[3)]	9	18
Total		40

[1)] Compensated by the hysteresis compensator in (8).
[2)] Fuzzy membership values μ.
[3)] Three "3 = D" cross products ($3 \times 3 = 9$ components).

experiments. Besides this device, various products are available, e.g., Mica series of Crossbow Company [22] or FlexStack of Boston Engineering [23].

GCFs are measured by the air pressure sensors in smart shoes and digitalized by analog-to-digital converters (ADC in Fig. 15) in real time. NI9201, an eight-channel/12-bit analog input module for CompactRio, served this function. The measured signals are filtered by the compensator in (8) and processed by the fuzzy logic to distinguish the gait phases. The outputs of the fuzzy logic are processed once again for the abnormality detection. Since the algorithms are programmed on field-programmable gate array (FPGA), they are processed in real time. The refined data are transferred to a host computer via direct memory access (DMA). CompactRio and the host computer were connected via a LAN cable, but many wireless options are available for the data transfer, e.g., Wi-Fi and Bluetooth. However, the limitation of bandwidth in wireless methods is a challenging issue.

Table IV shows the number of outputs of the proposed system. The system includes two sensor-embedded shoes, two identical fuzzy logics that detect the gait phases for each leg, and abnormality detection algorithms. The sampling rate and the data processing speed are 200 Hz. Note that this sampling rate does not need to be the same as that of the host computer.

B. GCF Patterns Measured by Smart Shoes

Fig. 16 shows motions for evaluating the performance of the smart shoe and its signal processing algorithms proposed in this paper. The subject was wearing the smart shoes and walking on a treadmill. The treadmill was velocity controlled such that the walking speed of the subject was constant (3.5 km/h). The subject was a healthy young male and imitated abnormal gaits as well as a normal gait. In Fig. 16(a), the subject was walking as usual, i.e., a normal gait. Note that the movements of the left leg match the gait phases shown in Fig. 9. Since the six

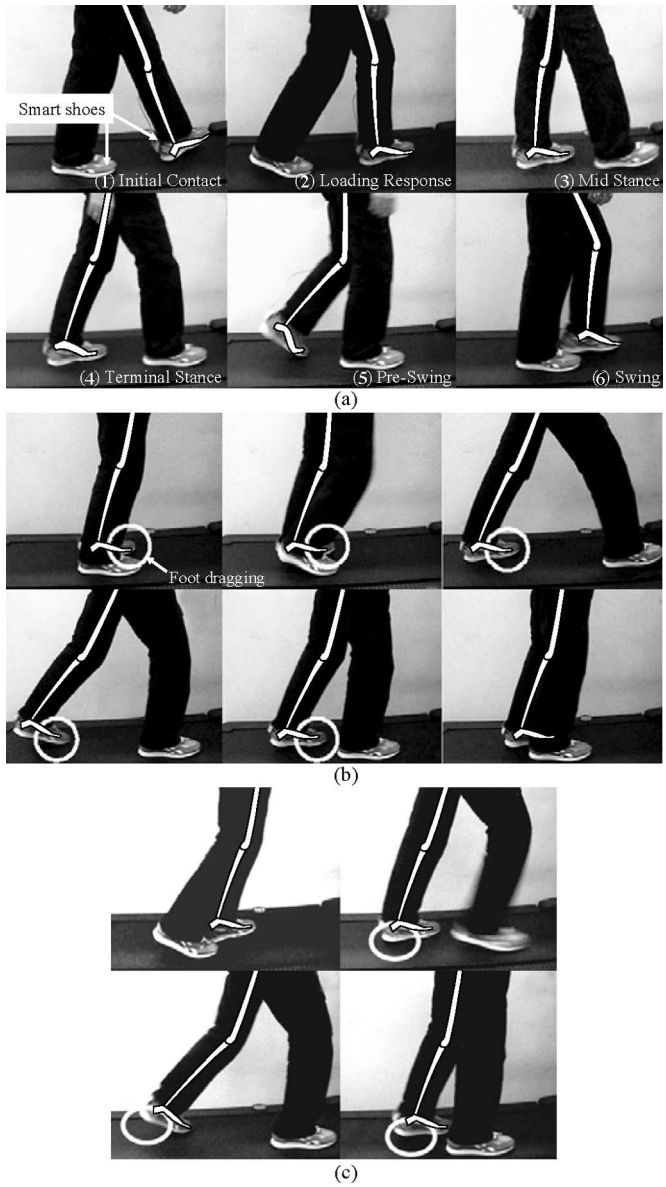

Fig. 16. Experimental motions for normal and abnormal gaits. (a) Normal gait motion: (1)–(6) match each gait phase shown in Fig. 9. (b) Abnormal gait motion with a foot dragging. (c) Abnormal gait motion without heel contact.

phases are clearly observed in the gait, the motions in Fig. 16(a) are to be detected as a normal gait by the proposed algorithms. In Fig. 16(b), the subject was acting as if his knee flexor is weak. As a result, his foot was dragging during swinging such that the toe touched the ground throughout the gait cycle. In Fig. 16(c), he acted as if he has a weak spastic paralysis on his ankle and knee, which results in an abnormal gait without heel contact.

Fig. 17 shows the GCF signals measured from the left foot and the gait phases detected during the experiment in Fig. 16(a). Note that the GCF signals have a certain pattern: sensors at Heel, Meta45, Meta12, and Toe show large GCFs sequentially. The locations of the sensors are as shown in Fig. 8(b). During swinging [e.g., see at 4 s in Fig. 17(a)], the foot was in the air, and therefore, the smart shoe did not measure any force. Note that the

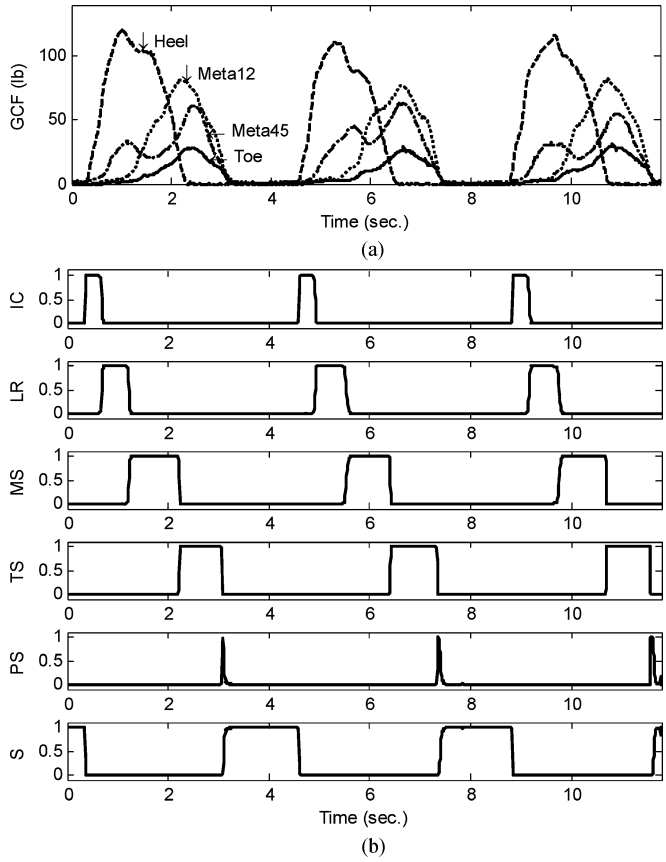

Fig. 17. GCF signals and gait phases in a normal gait. (a) GCF signals: locations of sensors are shown in Fig. 8(b). (b) Detected gait phases: IC, LR, MS, TS, PS, and S represent the FMVs of initial contact, loading response, mid stance, terminal stance, preswing, and swing phases, respectively.

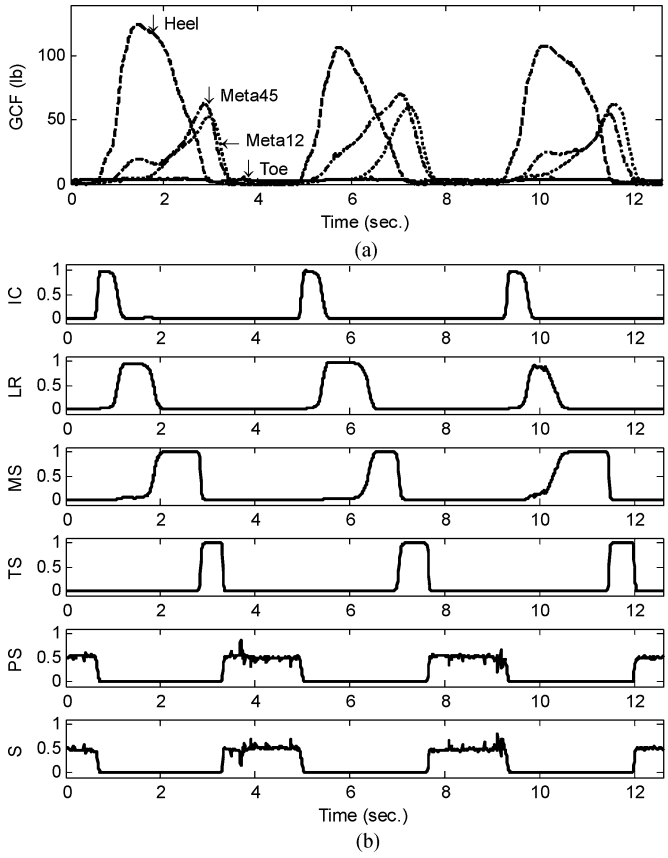

Fig. 18. GCF signals and gait phases in an abnormal gait with a foot dragging. (a) GCF signals. (b) Detected gait phases: Labels of y-axis are as in Fig. 17(b).

fuzzy logic detected the swing phase correctly at these times, as shown in Fig. 17(b), i.e., the FMV for the swing phase was close to one. Similarly, all the six phases were successfully detected by the fuzzy logic, and the detected phases were sequential because the subject followed a normal gait pattern.

Fig. 18 shows data measured during the experiment in Fig. 16(b), i.e., an abnormal gait with a foot dragging. Due to the foot dragging, the toe touches the ground continuously even in swing phases, and the sensor at toe measured small but continuous GCF, as shown in Fig. 18(a). Note that this abnormal motion can be observed in the gait phases detected by the fuzzy logic, as shown in Fig. 18(b). In the phases detected, the four phases that are not related to the toe (i.e., IC, LR, MS, and TS in the figure) were normal: they were detected sequentially. However, due to the problem at toe, the fuzzy logic determined the likelihoods of preswing and swing phases to have the medial values at the same time (e.g., see between 3 and 5 s in the figure). This might be because the GCF patterns could not be clearly analyzed by the expected patterns shown in Fig. 8.

Fig. 19 shows the results obtained by the experiment in Fig. 16(c), i.e., an abnormal gait without heel contact. In Fig. 19(a), the heel did not contact the ground throughout the experiment, while the other parts (i.e., Toe, Meta12, and Meta45) touched the ground. Due to the problem at heel, the subject hobbled and the magnitudes of GCFs in the left foot were relatively small compared with the other experiments shown in Figs. 17(a) and 18(a). In this experiment, the phases related to the heel, such as IC, LR, and MS in the figure, were not detected by the fuzzy logic. Since all the six phases are not sequentially observed by the fuzzy logic, the motions in Fig. 16(c) can be classified by an abnormal gait.

C. Detection of Abnormalities in GCF Pattern

The scaling factor of the fuzzy logic for each experiment is shown in Fig. 20. Fig. 20(a) shows the results during the normal gait experiment. The magnitude of the scaling factor was close to one except for at 7.2 s. This small spike is due to the preswing phase [see the same time in Fig. 17(b)]. In the subject's motions, duration of the preswing phase was too short that a sum of the unscaled FMVs at 7.2 s was less than one. However, the scaling factor was close to one most of the time, which implies that the measured GCF patterns were mostly explainable by the expected patterns in Fig. 9. Fig. 20(b) and (c) shows the results for abnormal gaits. Note that the scaling factor in Fig. 20(c) shows sometimes significantly large values. Therefore, the motions in Fig. 16(c) can be classified as an abnormal gait based on the scaling factor. However, it is hard to say that the scaling factor in Fig. 20(b) definitely observes the

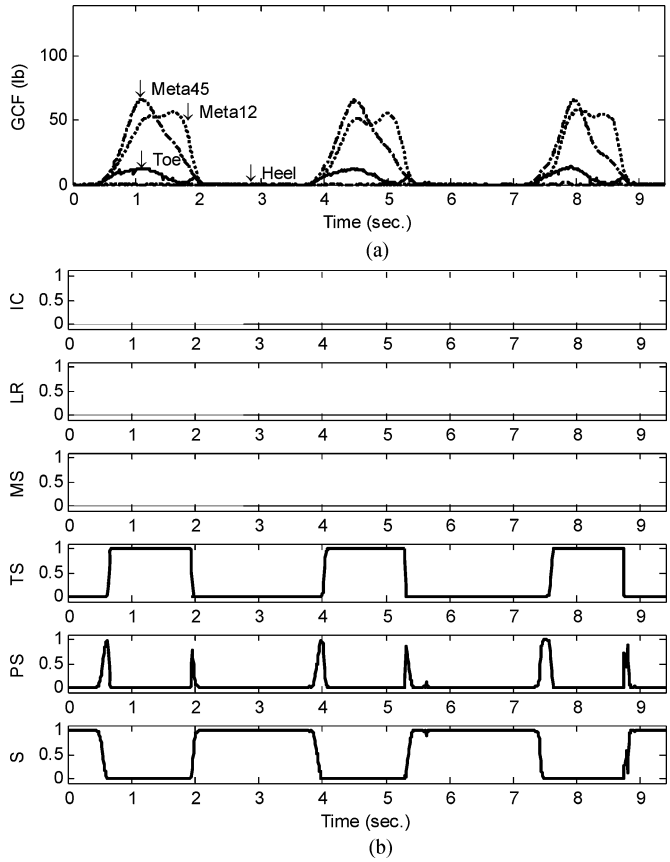

Fig. 19. GCF signals and gait phases detected for abnormal gait without heel contact. (a) GCF signals. (b) Detected gait phases: Labels of y-axis are as in Fig. 17(b).

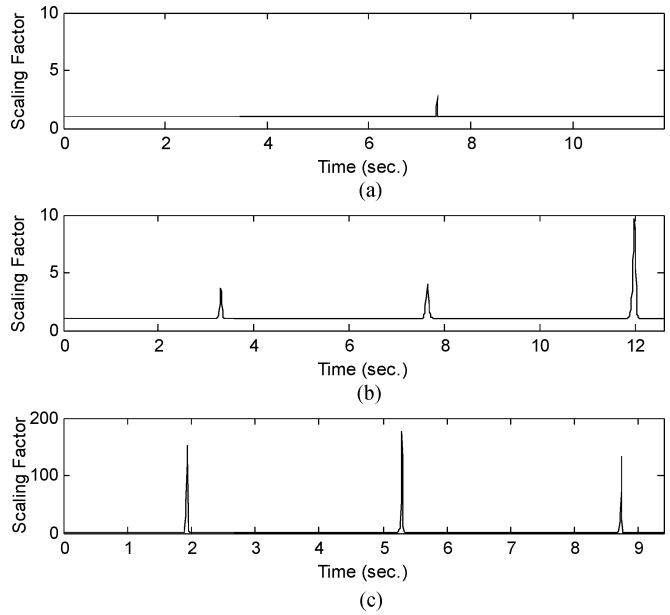

Fig. 20. Detection of abnormalities in GCF pattern. (a) Result for normal gait. (b) Result for abnormal gait with a foot dragging. (c) Result for abnormal gait without heel contact.

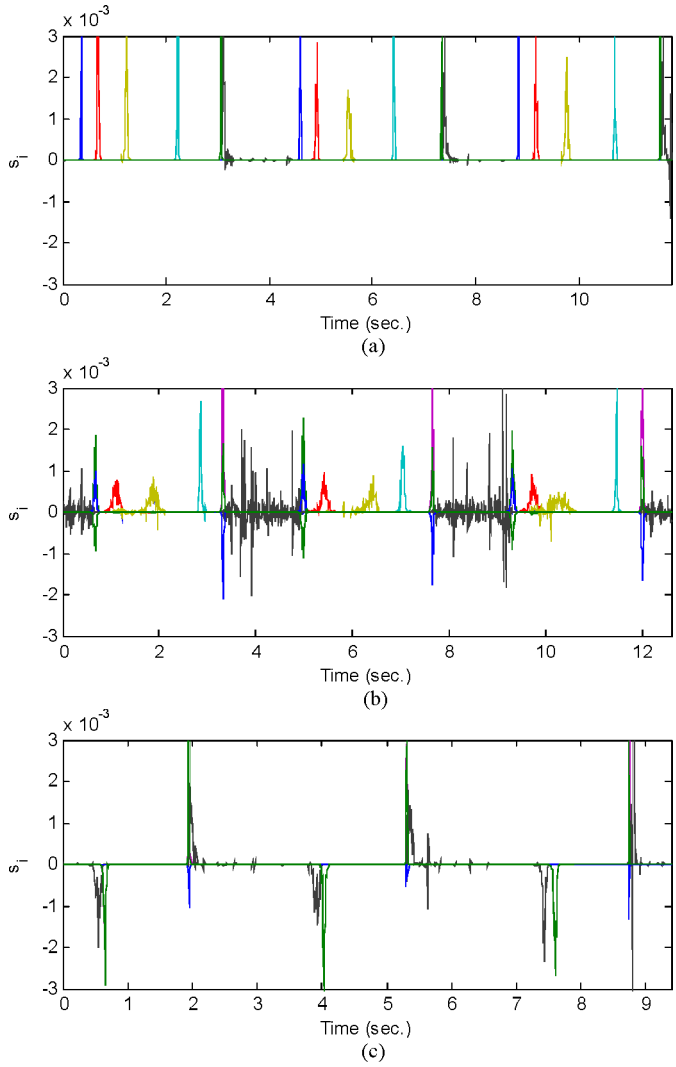

Fig. 21. Detection of abnormalities in sequence of gait phases. (a) Vector analysis result for a normal gait (no negative component shown). (b) Result for an abnormal gait with a dragging foot. (c) Result for abnormal gait without heel contact.

abnormality, because the scaling factor remains only modestly large. This is because the GCF patterns shown in Fig. 18(a) are analyzable with the GCF patterns expected in a normal gait, even though they are abnormal. Therefore, a complementary method is required to detect the abnormalities, which cannot be observed by the scaling factor.

D. Detection of Abnormalities in Gait Phase Sequence

The vector analysis in (13)–(21) provides complementary information for monitoring abnormalities in a human gait. As stated before, all of the components in the cross product of the gait phase vector and its time derivative [i.e., $\vec{s}'(k)$ in (14)] should be positive for all the time. Fig. 21 shows the results of the vector analysis for a normal gait shown in Fig. 16. In the figure, every component of $\vec{s}'(k)$ is plotted together. Fig. 21(a)–(c) corresponds to the experiments in Fig. 16(a)–(c), respectively. Note that the result for a normal gait [see Fig. 21(a)] does not

show large negative components for all the time, while those for abnormal gaits shown in Fig. 21(b)–(c) have negative values sometimes. The small negative components in Fig. 21(a) are because of the short duration of the preswing phase [see Fig. 17(b)]. However, the results in Fig. 21(b) show clearly observable negative values between 3 and 5 s, where the preswing phase was abnormally detected [see the same time in Fig. 18(b)]. Also, the results in Fig. 21(c) show negative values when the gait phases are abnormally detected in Fig. 19(b) [see 0.5, 4, and 7.5 s in both Figs. 19(b) and 21(c)]. At these times, the preswing phase appeared after the swing phase in Fig. 19(b), where the initial contact was supposed to have been appeared. Based on the vector analysis method proposed in this paper, motions in Fig. 16(b) and (c) can be classified as abnormal gaits. It should be noted that the vector analysis was available, because the gait phases were detected smoothly and continuously. Also, the smooth and continuous detection was possible, because the sensors for measuring GCFs in a shoe, i.e., the air pressure sensors with air bladders, showed good linearity with high resolution (i.e., low noise level). Therefore, the algorithms for detecting abnormalities in a human gait proposed in this paper are realizable using the proposed sensor-embedded shoes.

VI. Summary and Conclusion

In this paper, a gait monitoring system for motion phases and abnormalities in a human gait was introduced. The proposed system is constituted by three main parts: 1) a new sensor-embedded shoe that measures the GCFs; 2) an algorithm that detects motion phases from the measured signals; and 3) a higher level algorithm that evaluates the degree of abnormalities in the detected motion phases.

The proposed sensor-embedded shoe called a smart shoe has four sensing units in the sole of the shoe. Each sensing unit consists of an air bladder and an air pressure sensor. When the contact force is exerted by a foot, the air bladder is deformed and the inside pressure change is measured by the pressure sensor. The performance of the proposed sensing unit was verified by experiments. For compensation of the measured signals, a digital filter was designed based on a physical model of the air bladder.

A method for detecting motion phases in a human gait from the measured signals was designed based on the fuzzy logic in this paper. The outputs of the proposed method were related to the likelihood of each phase. Since the motion phases in a human gait changes smoothly and continuously, an algorithm was designed such that the gait phases were detected smoothly and continuously. Also, the scaling factor in the proposed method was related to the degree of abnormalities in the gait.

In addition to the phase detection algorithm, a higher level algorithm that monitors abnormalities in the detected gait phases was proposed in this paper. The proposed method deals with the gait phases as a vector and detects abnormalities in a gait phase transition by monitoring the path of the vector. The results obtained by the vector analysis method and the scaling factor in the fuzzy logic are complementary. The proposed methods were verified by experiments.

The abnormality detection method in this paper utilized the gait phases detected by the fuzzy logic for each foot. The proposed methods are under clinical verification in the University of California, San Francisco. In future works, an algorithm that observes gait abnormalities based on the signals and/or the detected phases from both feet will be introduced. It is expected that such algorithm helps identify additional gait abnormalities.

References

[1] J. Perry, *Gait Analysis*. Thorofare, NJ: SLACK, Inc., 1992.
[2] (2009, Mar.). [Online]. Available: http://www.hocoma.ch.
[3] T. Hayashi, H. Kawamoto, and Y. Sankai, "Control method of robot suit HAL working as operator's muscle using biological and dynamical information," in *Proc. IEEE/RSJ Int. Conf. Intell. Robots Syst. (IROS 2005)*, pp. 3063–3068.
[4] J. Blaya and H. Herr, "Adaptive control of a variable-impedance ankle-foot orthosis to assist drop-foot gait," *IEEE Trans. Rehabil. Eng.*, vol. 12, no. 1, pp. 24–31, Mar. 2004.
[5] K. Kong and D. Jeon, "Design and control of an exoskeleton for the elderly and patients," *IEEE/ASME Trans. Mechatronics*, vol. 11, no. 4, pp. 428–432, Aug. 2006.
[6] M. C. Carrozza, A. Persichetti, C. Laschi, F. Vecchi, R. Lazzarini, P. Vacalebri, and P. Dario, "A wearable biomechatronic interface for controlling robots with voluntary foot movements," *IEEE/ASME Trans. Mechatronics*, vol. 12, no. 1, pp. 1–11, Feb. 2007.
[7] W. Ye, Y. Xu, and K. K. Lee, "Shoe-Mouse: An integrated intelligent shoe," in *Proc. IEEE/RSJ Int. Conf. Intell. Robots Syst. (IROS 2005)*, pp. 1163–1167.
[8] NoHands mouse. (2009, Mar.). [Online]. Available: http://www.footmouse.com.
[9] S. J. M. Bamberg, A. Y. Benbasat, D. M. Scarborough, D. E. Krebs, and J. A. Paradiso, "Gait analysis using a shoe-integrated wireless sensor system," *IEEE Trans. Inf. Technol. Biomed.*, vol. 12, no. 4, pp. 413–423, Jul. 2008.
[10] B. Huang, M. Chen, X. Shi, and Y. Xu, "Gait event detection with intelligent shoes," in *Proc. IEEE Int. Conf. Inf. Acquisition (ICIA 2007)*, pp. 579–584.
[11] M. Chen, B. Huang, and Y. Xu, "Intelligent shoes for abnormal gait detection," in *Proc. IEEE Int. Conf. Robot. Autom. (ICRA 2008)*, pp. 2019–2024.
[12] I. P. I. Pappas, M. R. Popovic, T. Keller, V. Dietz, and M. Morari, "A reliable gait phase detection system," *IEEE Trans. Neural Syst. Rehabil. Eng.*, vol. 9, no. 2, pp. 113–125, Jun. 2001.
[13] M. Kothari, J. G. Webster, W. J. Tompkins, J. J. Wertsch, and P. Bach-Y-Rita, "Capacitive sensors for measuring the pressure between the foot and shoe," in *Proc. IEEE Annu. Int. Conf. Eng. Med. Biol. Soc.*, 1988, vol. 2, pp. 805–806.
[14] M. A. Razian and M. G. Pepper, "Design, development, and characteristics of an in-shoe triaxial pressure measurement transducer utilizing a single element of piezoelectric copolymer film," *IEEE Trans. Neural Syst. Rehabil. Eng.*, vol. 11, no. 3, pp. 288–293, Sep. 2003.
[15] BDSX pressure sensor. (2009, Mar.). [Online]. Available: http://sensortechnics.com.
[16] FC21 loadcell. (2009, Mar.). [Online]. Available: http://msisensors.com.
[17] N. E. Dowling, *Mechanical Behavior of Materials*, 2nd ed. Englewood Cliffs, NJ: Prentice-Hall, 1999.
[18] P. M. Larsen, "Industrial applications of fuzzy logic control," *Int. J. Man–Mach. Stud.*, vol. 12, no. 1, pp. 3–10, 1980.
[19] K. Tanaka, *An Introduction to Fuzzy Logic for Practical Applications*. New York: Springer-Verlag, 2007.
[20] Z. K. Silagadze, "Multi-dimensional vector product," *J. Phys. A: Math. Gen.*, vol. 35, pp. 4949–4953, 2002.
[21] (2009, Mar.). [Online]. Available: http://www.ni.com/compactrio
[22] (2009, Mar.). [Online]. Available: http://xbow.com
[23] (2009, Mar.). [Online]. Available: http://www.boston-engineering.com
[24] D. Winter, *Biomechanics and Motor Control of Human Movement*. New York: Wiley, 1990.

Kyoungchul Kong (S'04) received the B.Eng. degree (*summa cum laude*) in mechanical engineering and the B.S. degree in physics, in 2004, and the M.S. degree in mechanical engineering in 2006, all from Sogang University, Seoul, Korea. He is currently working toward the Ph.D. degree in mechanical engineering at the University of California, Berkeley.

He has authored or coauthored more than 30 technical articles published in journals and conference proceedings. His current research interests include design, modeling, and control of mechatronic systems with emphasis on betterment of quality of human life.

Mr. Kong was the recipient of the Best Student Paper Award of the IEEE Conference on Advanced Intelligent Mechatronics (AIM) in 2008, the Best Paper Award from the Division of Dynamic Systems and Control of the Korean Society of Mechanical Engineers (KSME) Annual Conference in 2005, and the Best Poster Award of the 3rd Center of Intelligent Robot Workshop in 2005. Also, he was the finalist of the Best Student Paper at the IEEE Advanced Intelligent Mechatronics (AIM) Conference in 2005 and the Best Poster Paper at the International Federation of Automatic Control (IFAC) World Congress in 2008.

Masayoshi Tomizuka (M'86–SM'95–F'97) was born in Tokyo, Japan, in 1946. He received the B.S. and M.S. degrees from Keio University, Tokyo, Japan, in 1968 and 1970, respectively, and the Ph.D. degree from Massachusetts Institute of Technology, Cambridge, all in mechanical engineering.

In 1974, he joined the Department of Mechanical Engineering, University of California, Berkeley, where he is currently the Cheryl and John Neerhout Jr. Distinguished Professor Chair. His current research interests include optimal and adaptive control, digital control, signal processing, motion control, and control problems related to robotics, machining, manufacturing, and information storage devices and vehicles.

Prof. Tomizuka was the Editor-in-Chief of the IEEE/ASME TRANSACTIONS ON MECHATRONICS from 1997 to 1999. He was the General Chairman of the 1995 American Control Conference and was the President of the American Automatic Control Council during 1998 and 1999. He is a Fellow of the ASME and the Society of Manufacturing Engineers. He was the recipient of the Best J-DSMC Best Paper Award (1995), the Dynamic Systems and Control Division (DSCD) Outstanding Investigator Award (1996), the Charles Russ Richards Memorial Award (ASME, 1997), the Rufus Oldenburger Medal (ASME, 2002), and the John R. Ragazzini Award (2006). He was the Technical Editor of the *American Society of Mechanical Engineers (ASME) Journal of Dynamic Systems, Measurement and Control (J-DSMC)* (1988–1993). He has also been an Associate Editor of the *Journal of the International Federation of Automatic Control, Automatica*, and *European Journal of Control*.